Fast Characterization of Moving Samples with Nano-Textured Surfaces

Madsen, Morten Hannibal; Hansen, Poul-Erik; Zalkovskij, Maksim; Karamehmedovi, Mirza; Garnæs, Jørgen

Published in:
Optica

Link to article, DOI:
10.1364/OPTICA.2.000301

Publication date:
2015

Document Version
Publisher's PDF, also known as Version of record

optica

Fast characterization of moving samples with nano-textured surfaces

Morten Hannibal Madsen,[1,*] Poul-Erik Hansen,[1] Maksim Zalkovskij,[2] Mirza Karamehmedović,[3] and Jørgen Garnæs[1]

[1]Danish Fundamental Metrology A/S, Matematiktorvet 307, 2800 Kgs. Lyngby, Denmark

[2]NIL Technology ApS, Diplomvej 381, 2800 Kgs. Lyngby, Denmark

[3]Department of Applied Mathematics and Computer Science & Department of Physics, Technical University of Denmark, Matematiktorvet 303B, DK-2800 Kgs. Lyngby, Denmark

*Corresponding author: mhm@dfm.dk

Received 13 October 2014; revised 25 February 2015; accepted 26 February 2015 (Doc. ID 224753); published 30 March 2015

Characterization of structures using conventional optical microscopy is restricted by the diffraction limit. Techniques such as atomic force and scanning electron microscopy can investigate smaller structures but are very time consuming. We show that using scatterometry, a technique based on optical diffraction, integrated into a commercial light microscope we can characterize nano-textured surfaces in a few milliseconds. The adapted microscope has two detectors, a CCD camera used to easily find an area of interest and a spectrometer for the measurements. We demonstrate that the microscope has a resolution in the nanometer range for the topographic parameters—height, width, and sidewall angle of a periodic grating—even in an environment with many vibrations, such as a production facility with heavy equipment.

OCIS codes: (050.0050) Diffraction and gratings; (110.0180) Microscopy; (120.4570) Optical design of instruments; (120.5820) Scattering measurements; (290.3700) Linewidth; (100.3200) Inverse scattering.

http://dx.doi.org/10.1364/OPTICA.2.000301

1. INTRODUCTION

An increasing number of products utilizing micro/nano-textured surfaces are moving toward the commercial market. However, most conventional characterization techniques are inapplicable in a large-scale industrial environment. Imaging techniques such as atomic force microscopy (AFM), scanning electron microscopy (SEM), and confocal imaging are all very sensitive to vibrations. Isolation and damping of vibrations is a cumbersome task, if possible at all [1]. Thus, there is a high demand for new *in situ* imaging techniques, especially in a production environment. Furthermore, the above-mentioned characterization techniques are all highly time consuming, which restricts their applicability in a large-scale industrial process flow.

In this paper we introduce an adapted optical microscope capable of measuring with resolution in the nanometer range on a moving sample. The system is based on the principles of optical diffraction microscopy (ODM), where the spectrum of the reflected light is studied [2,3]. The scattering intensities are independent of the sample movement, as long as one observes an area with uniform structures. We show that one can shake the microscope or move the sample during acquisition without affecting the results of the measurements. This allows our adapted optical microscope to be integrated in a production line, to perform, e.g., quality control in the nanoscale range.

Several types of scatterometers exist, including ODM [2–4], angular scatterometry [5–7], the Fourier lens system [8], coherent Fourier scatterometry [9–11], white light interference Fourier scatterometry [12], and naked-eye observations [13]. Two general challenges for scatterometry are imaging small areas and finding a specific area of interest. In this paper, we demonstrate a method to overcome both of these challenges

by building the scatterometer into a conventional optical microscope. Furthermore, the spot size, which defines the imaged area, can easily be controlled by change of objective. Typical spot sizes are in the range from less than 100 μm to several millimeters.

The scatterometer technique is suitable for structures that can be modeled using periodic or nonperiodic boundary conditions. Periodic structures include one-dimensional (1D) gratings and two-dimensional (2D) arrays of structures. Both types of structures with dimensions in the micro/nano-range are entering the consumer market, hence the need for fast and reliable characterization methods. Gratings with 1D nanostructures are used, e.g., for structural colors in the design of surfaces with iridescence [14,15]. An AFM image of a 1D grating and typical topography parameters of interest are shown in Fig. 1. Nanowire-based solar cells [16] are typically fabricated in a well-ordered 2D array [17]. As these devices are also approaching the market, methods for fast large-area characterization with nanometer resolution are needed. The optical response for different crystal orientations [18] and the angle-dependent absorption [19] for nanowires have recently been measured, paving the road for the topographical measurements. Nonperiodic boundary conditions can, for instance, be used to model photonic crystal waveguides, Bragg mirrors, grating couplers [20], and single structures such as microfluidic channels and submicrometer wires [21].

2. EXPERIMENTAL SETUP

The system, shown in Fig. 2, is based on a Navitar optical microscope (12× zoom) equipped with a 5 W LED light source

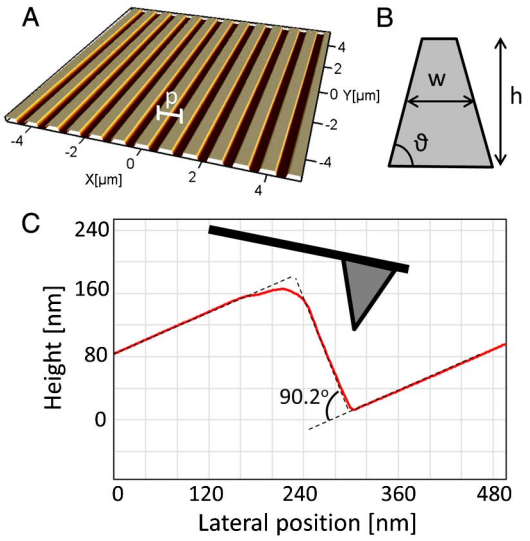

Fig. 1. 1D grating in Si(100). A, topographic AFM image of a 1D grating with a pitch, p, of 800 nm. All axes have the same length scale. B, sketch of a single structure seen from the side. The definitions of the height, h, width, w, and sidewall angle, ϑ, are indicated in the figure. The filling factor is defined as the amount of material present compared to a uniform film with the same thickness as the height of the nanostructures. C, profile obtained with a tilted sample 23° in the AFM of the grating with a 1400 nm pitch. The shape and angle of the scanning AFM tip are indicated in the figure.

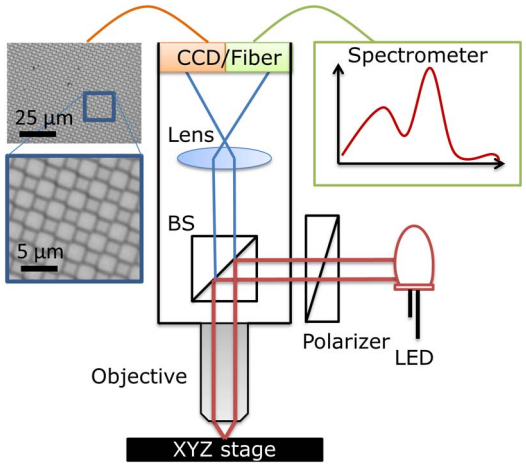

Fig. 2. Sketch of experimental setup. Data acquisition can be performed using either a CCD camera or a spectrometer. The images to the left show a calibration artifact with 3 μm pitch acquired with a 50× objective. CCD, charge-coupled device (1.3 MPx); LED, light emitting diode (5 W); BS, beam splitter cube (50/50).

(Navitar coaxial LED illuminator), a linear polarizer, and a monochrome 1.3 megapixel (MPx) CCD camera. The CCD camera is interchangeable with a lens system and a spectrometer (Ocean Optics USB-2000), which has been calibrated using a low-pressure krypton calibration light source with traceable spectral lines. The microscope is equipped with infinity-corrected objectives with magnifications in the range of 5×–50×. In another setup, the microscope is adapted by introducing a second beam splitter cube (50/50) just over the objective, and one of the beams is focused into a fiber connected to a spectrometer. A more detailed description of this system can be found in the Supplement 1. In such a configuration one can obtain the image and spectrum simultaneously, but at the cost of about four times reduction in intensity.

The focus can be adjusted by either moving the lower part of the objective or moving the sample stage, but in general, only the sample stage is used for focusing. The sample is brought into focus by monitoring it on the CCD detector, which is a huge advantage over other scatterometry setups, where one often struggles with finding the area of interest and bringing it in focus. Often the focus point is found on scatterometers by finding the maxima for the intensity of the spectrum, which is not a very reliable method. The CCD is also used to estimate the effective spot size for the different objectives by measuring on calibration artifacts. With the 5× objective the spot size is 1.5 mm, with the 27× objective the spot size has a diameter of 250 μm, and with the 50× objective the spot size is 125 μm.

A reference and a dark spectrum are acquired before measuring the sample of interest. The reference spectrum, $I_{\mathrm{ref}}(\lambda)$, is acquired on a surface with known reflection coefficients, e.g., a Si(100) substrate. The acquisition time is set to take full advantage of the dynamic range of the spectrometer. A typical acquisition time is 5 ms, which is then kept constant for this study. Second, a dark spectrum, $I_{\mathrm{dark}}(\lambda)$, is acquired by removing the reference sample. The dark spectrum corrects for noise

in the spectrometer and eventual ambient light conditions that give a constant signal. The diffraction efficiencies are calculated for each wavelength using

$$\eta(\lambda) = \frac{I_{\text{sample}}(\lambda) - I_{\text{dark}}(\lambda)}{I_{\text{ref}}(\lambda) - I_{\text{dark}}(\lambda)} R(\lambda), \quad (1)$$

where $R(\lambda)$ are the reflection coefficients of the reference sample.

To simplify the modeling only the zeroth-order reflection is measured. This gives rise to the following constraint on the grating period d:

$$d \lesssim \frac{\lambda_{\text{min}}}{2\ \sin(2\theta_{\text{NA}})}. \quad (2)$$

Here, λ_{min} is the minimum wavelength measured with the spectrometer and θ_{NA} is the collection angle for an objective with numerical aperture NA $= \sin(\theta_{\text{NA}})$ in air. In contrast to conventional imaging, it is thus favorable to use an objective with a low numerical aperture, and for the measurements presented in this study we use a 5× objective with NA $= 0.14$. For this objective and with the cut-off wavelength $\lambda_{\text{min}} = 445$ nm, we find that the period of the grating should be less than 803 nm to prevent first-order reflections from being imaged. However, as demonstrated experimentally in this paper, first-order reflections can to a good approximation also be omitted in the simulations for gratings with a larger pitch.

3. INVERSE MODELING

The data analysis is based on an inverse-modeling approach in which scattering intensities are modeled first and afterwards compared to the experimental values. The scattering intensities are calculated using the rigorous coupled-wave analysis (RCWA) method as described in Refs. [22] and [23]. The periodic grating is divided into slabs, for which the scattering is modeled individually, and then the scattering from each slab is coupled through boundary conditions. A database including variations in height, filling factor, and sidewall angle is modeled for each pitch $\alpha = (\alpha_{\text{height}}, \alpha_{\text{FF}}, \alpha_{\text{sw}})$. Other methods for modeling, such as finite element analysis, can also be used, but are significantly slower. For ODM many wavelengths are needed for each model, and hence the computation time is very long using finite element methods. All models, regardless of the used method, require prior knowledge of the index of refraction and the extinction coefficients of the considered materials. Based on our experience with the system we have found that the optical properties should be known within a few percent to achieve a good reconstruction.

As a regularizing measure, the modeled scattering intensities are stored in a database and then compared with the experimental data using a least-squares optimization as a gauge for the quality of the fit:

$$\chi^2 = \sum_{i=1}^{N} \left[\frac{\eta - f_i(\alpha)}{\sigma_i}\right]^2. \quad (3)$$

Here σ_i are the uncertainties on the experimental data as described in Ref. [4], and $f_i(\alpha)$ are the modeled scattering intensities for the ith element with the shape α. The standard uncertainty vectors, σ_i, depend on the measured parameters $I_{\text{grating}}(\lambda)$, $I_{\text{ref}}(\lambda)$, and $I_{\text{background}}(\lambda)$, and are calculated from the error propagation of $\eta(\lambda)$. Low uncertainties on the experimental data are achieved for $I_{\text{background}}(\lambda) \ll I_{\text{grating}}(\lambda)$ and by averaging of the signals. The database element with the lowest χ^2 value is the best match to the model. From Eq. (3) it can be seen that experimental data points with an associated large uncertainty give a smaller contribution to the sum than data points with a relatively small uncertainty. Thus, the best model is found with the most weight on the data points with the smallest uncertainty.

For increased precision, the parameters of the best-fit model are further optimized with a linear fit using neighbor diffraction efficiencies. The optimization is also used to estimate the uncertainty on the fitted parameters. It has also been demonstrated that one can use a two-step optimization procedure, where first a global and then a local optimization are applied [24].

For validation of the system a set of thin-film transfer standards has been measured with the scatterometer. The transfer standards consist of SiO_2-coated Si(100) substrates, where the SiO_2 has a thickness in the range of 6 nm to 1 μm. Optical constants for input to the simulations are obtained from [25]. The results are summarized in Table 1, and experimental data and fit can be found in Supplement 1. The confidence limits for the scatterometry fits are found using constant chi-square boundaries [26]. For ν degrees of freedom the chi-square distribution $\Delta\chi^2_\nu = \chi^2_\nu - \chi^2_{\text{min}}$ is found, where χ^2_{min} is the global minimum of the chi-square distribution. To find the confidence limit of a single parameter, $\nu = 1$, with a confidence interval of 95%, the relation $\Delta\chi^2_\nu < 4$ should be fulfilled. It should be stressed that the confidence limit only gives an uncertainty estimate of the parameters included in the analysis. It is seen from the data in Table 1 that the scatterometer measures a value within the expanded uncertainty interval of the transfer standards for thicknesses above 160 nm. For thicknesses less than 160 nm the visible wavelength spectrum of

Table 1. Thin-Film Measurements on Transfer Standards[a]

Reference [nm]	Scatterometer [nm]
6.0 ± 1.1	11 ± 8
69.7 ± 1.3	72 ± 4
163.2 ± 1.5	162 ± 4
386.4 ± 2.3	387 ± 2
1003.0 ± 5.1	1002 ± 2

[a]The reference values are measured using traceable spectroscopic ellipsometry, and ± denotes the expanded standard uncertainty ($k = 2$) equivalent to a confidence interval of 95%. For the scatterometer data ± denotes the 95% confidence interval of the fit. For transfer standards with thickness above 160 nm the scatterometer measures the thickness within the standard uncertainty of the certified reference measurements.

diffraction efficiencies is a monotone curve that increases the confidence limits on the fit to the measurements.

4. SAMPLE WITH NANO-TEXTURED SURFACE

For tests of the instrument on nano-textured surfaces a multi-period 1D silicon sample with eight gratings was fabricated. The grating patterns were defined by deep ultraviolet lithography, with grating periods ranging from 700 to 1400 nm in steps of 100 nm. After development of the resist, the pattern was transferred to a silicon substrate by the use of inductively coupled plasma etching, where C_4F_8 and SF_6 gasses were used.

For reference characterization of the height, pitch, and sidewall angle, three different techniques had to be used. Additional experimental data can be found in Supplement 1. The height was characterized using a traceable NX20 atomic force microscope (AFM) from Park Instruments and analyzed using the step height module in the SPIP software package (Image Metrology) for each individual line in the image. For the area with a 800 nm pitch the height was found to be $h = 189.1$ nm with an expanded standard uncertainty ($k = 2$) of $U(h) = 1.3$ nm.

The filling factor of the grating is challenging to measure with an AFM. One has to take both the tip shape and the edge shape of the grating into account [4]. Instead, the width analysis is based on SEM images. Accurate measurements with an SEM are challenged by several limitations based upon the interaction of the electron beam with the sample [27]. A detailed analysis of these factors is outside the scope of this paper, but we have omitted the demand for accurate calibration of the microscope itself by performing a relative measurement to estimate the filling factor. For the area with 800 nm pitch, the filling factor of the 1D grating was found to be FF = 0.477, roughly equivalent to a width of the structures of 382 nm. The uncertainty on the SEM measurements of the filling factor has been estimated to 0.007.

Measurements of the angles of the sidewalls are unreliable using normal AFM and SEM methods. Instead the sample was measured by an intermittent contact mode (tapping mode) AFM with the sample tilted 23° as shown in Fig. 1C. Profiles were now recorded perpendicular to the grooves, and the sidewall angle was estimated from four to six grooves on the average profile of the x gradient. The sidewall angle could now be measured without having to correct for the tip shape and was found to be $\vartheta = 90.1°$ with an associated expanded uncertainty of $U(\vartheta) = 1.5°$ for the grating with a 800 nm pitch.

5. SCATTEROMETRY MEASUREMENTS

All gratings on the silicon sample were measured with the scatterometer, and a blank area on the same Si(100) substrate was used for the reference measurement. Before performing the measurements the area of interest was located using the CCD camera and brought into focus by adjusting the height. Measurement results for the area with 800 nm pitch obtained with TE-polarized light are shown in Fig. 3, and data for other areas can be found in Supplement 1. TE-polarized light has been chosen as the simulations using RCWA are faster than for TM-polarized light [28]. Experimental data have been

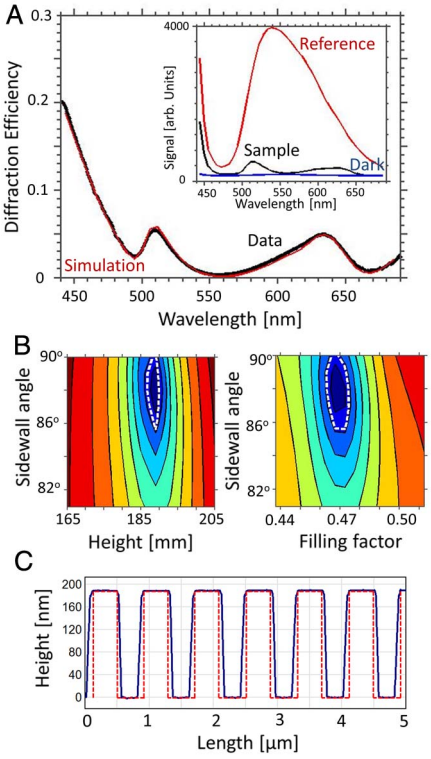

Fig. 3. Scatterometry measurements for TE-polarized light on a 1D grating with a period of 800 nm etched in Si(100). A, experimental data (black curve) and simulation for best fit (red curve) of diffraction efficiency. The best fit is found for the parameters $h = 189$ nm, FF = 0.468, and $\alpha = 88°$. The inset shows the raw data for the sample, dark, and reference spectra. B, color plots of the χ^2 values. Dark blue shows areas with the lowest χ^2 value and hence the parameters for the best fit. The dashed white curve indicates the 95% confidence interval of the fit. C, profile of the best-fit data (red dashed curve) overlayered on experimental data obtained with an atomic force microscope (blue solid curve). Due to tip convolution the AFM profile overestimates the width and sidewall angle.

obtained for the wavelength range from 445 to 690 nm and smoothed using a second-order Savitzky–Golay filter [29] with a frame size of 11 points. The limited wavelength range is due to antireflective coating of the optical components in the Navitar microscope system.

The confidence limits for the fitting parameters can be treated individually [26], and thus the relation should be fulfilled. The χ^2 values are plotted for both the constant filling factor (FF = 0.468) and the constant height ($h = 189$ nm) in Fig. 3B. The white dashed line indicates $\Delta\chi^2_\nu = 4$ and hence the 95% confidence interval of the fit. For the height, filling factor, and sidewall angle the 95% confidence interval is found to be 2 nm, 0.005, and 3°, respectively. In Fig. 3C the profile from an AFM scan (solid blue line) has been overlayered with a profile of the best-fit data (dashed red line). It is seen that the AFM overestimates the width and sidewall angle of the structures due to the tip convolution.

Scatterometry and reference measurement results for all gratings with pitches in the range of 700–1400 nm are shown in Fig. 4. The figure shows the obtained heights, fill factors, and

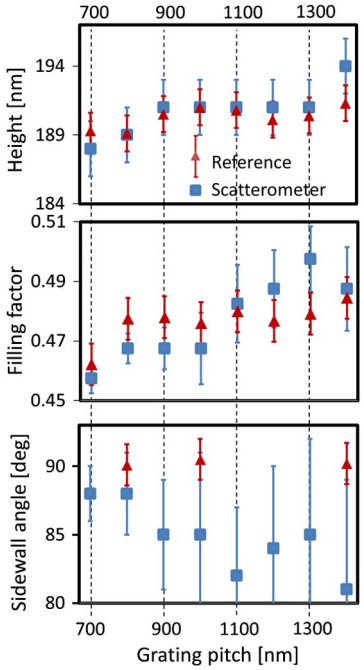

Fig. 4. Height, fill factor, and sidewall angle data with 2σ confidence limits for the different gratings. The scatterometry data are most accurate for pitches below 800 nm, as no higher-order reflections are collected when observing these structures. The reference measurements are obtained with AFM, SEM, and tilted AFM for the height, filling factor, and sidewall angle, respectively.

sidewall angles with 2σ confidence limits. For pitches in the range from 700 to 1200 nm there is excellent agreement on the height and fill factor values for the different methods. For pitches above 1200 nm the agreement is worse due to the fact that the scatterometer collects a significant amount of signal from higher diffraction orders and that this contribution is not included in the scatterometry data analysis.

The sidewall angles have only been measured with AFM for the gratings with 800, 1000, and 1400 nm pitch, but as all structures have been dry etched in the same process, we therefore expect the sidewall angle to be close to the same value for all pitches. The scatterometry sidewall angles with pitches at 800 nm or below are within the 2σ confidence limits, whereas the sidewall angles for pitches above 800 nm are not. This clearly shows that the sidewall angle is the most sensitive parameter to the collection of signal from higher diffraction orders.

6. MOVING THE SAMPLE

An advantage with the scatterometry setup is that the measurements are very robust to vibrations. This is demonstrated by moving the sample during data acquisition and summarized in Table 2. The sample was translated about 100 μm/s in either the x or y direction during data acquisition. Such a movement makes the optical image extremely blurry, but has no effect on the scattering intensities, as we still measure inside the same field on the sample. Please note that both the microscope and/or the sample can be moved during acquisition, thus making the microscope suitable to be used in a production environment.

Table 2. Measurements on a 1D Grating with a Pitch of 800 nm Etched in a Si(100) Substrate[a]

Method	Height [nm]	Filling Factor	Sidewall Angle [°]
AFM	189.1 ± 1.3	N/A	N/A
SEM	N/A	0.477 ± 0.007	N/A
Tilted AFM	N/A	N/A	90.1 ± 1.5
Scatterometer	189 ± 2	0.468 ± 0.005	88 ± 3
Scat., moving sample	189 ± 2	0.468 ± 0.005	87 ± 3
Scat., defocused +10 mm	189 ± 2	0.469 ± 0.005	88 ± 3
Scat., defocused −10 mm	188 ± 4	0.470 ± 0.007	87 ± 3

[a]Three different techniques have to be applied for reference measurements of the height, filling factor, and sidewall angle of the grating, whereas the scatterometer can measure all these in a single measurement. Moving the sample during acquisition has no effect on the scatterometry measurements, as long as one measures inside a homogeneous area. The effect of defocusing has been tested with the 5× objective.

Defocusing is detrimental for obtaining images in the image plane. However, with the scatterometer, only a very small effect on the measured values is seen, even for a defocus of 10 mm with the 5× objective. For other objectives with lower working distance the effect of defocusing is larger. Again, the sample can be moved in the z direction during acquisition without affecting the outcome of the measurements, as long as the movement is less than 10 mm when using the 5× objective.

For the scatterometer to be integrated in an industrial production line, one will also have to take the rotation of the sample into account. For TE measurements the polarization of the incoming light should be aligned with the grating direction. We have shown that for the 800 nm grating rotations less than 6° gives rise to an uncertainty of less than 2 nm in the height, 0.005 for the filling factor, and 3° for the sidewall angle. More details can be found in Supplement 1.

7. CONCLUSION

In conclusion, we have demonstrated that by simple adaptions to an optical microscope we can measure nano-textured surfaces with a resolution in the nanometer range. The microscope has been validated by measuring on certified transfer artifact and 1D gratings with pitches in the range from 700 to 1400 nm. The measurements are very robust, such that vibrations of the sample and/or the microscope do not affect the results. The sample can be translated during acquisition, as long as the beam spot is kept inside an area with homogenous structures, which makes the proposed microscope well suited for implementation in a production environment.

FUNDING INFORMATION

Danish National Advanced Technology Foundation (NanoPlast); The Danish Council for Strategic Research (Polynano); The European Union: Theme NMP.2012.1.4-3 (309672).

See Supplement 1 for supporting content.

REFERENCES

1. R. Leach, *Fundamental Principles of Engineering Nanometrology* (Elsevier, 2014).
2. X. Niu, N. Jakatdar, J. Bao, and C. Spanos, "Specular spectroscopic scatterometry," IEEE Trans. Semicond. Manuf. **14**, 97–111 (2001).
3. N. Agersnap, P.-E. Hansen, J. C. Petersen, J. Garnaes, N. Destouches, and O. Parriaux, "Critical dimension metrology using optical diffraction microscopy," Proc. SPIE **5985**, 68–78 (2005).
4. J. Garnaes, P.-E. Hansen, N. Agersnap, J. Holm, F. Borsetto, and A. Kuhle, "Profiles of a high-aspect-ratio grating determined by spectroscopic scatterometry and atomic-force microscopy," Appl. Opt. **45**, 3201–3212 (2006).
5. D.-M. Shyu, Y.-S. Ku, and N. Smith, "Angular scatterometry for linewidth roughness measurement," Proc. SPIE **6518**, 65184G (2007).
6. A. Kato and F. Scholze, "Effect of line roughness on the diffraction intensities in angular resolved scatterometry," Appl. Opt. **49**, 6102–6110 (2010).
7. O. Paul, F. Widulle, B. H. Kleemann, and A. Heinrich, "Nanometrology of periodic nanopillar arrays by means of light scattering," Proc. SPIE **8788**, 87881O (2013).
8. P. Boher, J. Petit, T. Leroux, J. Foucher, Y. Desieres, J. Hazart, and P. Chaton, "Optical Fourier transform scatterometry for LER and LWR metrology," Proc. SPIE **5752**, 192–203 (2005).
9. J. P. Ogilvie, E. Beaurepaire, A. Alexandrou, and M. Joffre, "Fourier-transform coherent anti-Stokes Raman scattering microscopy," Opt. Lett. **31**, 480–482 (2006).
10. S. Roy, N. Kumar, S. Pereira, and H. Urbach, "Interferometric coherent Fourier scatterometry: a method for obtaining high sensitivity in the optical inverse-grating problem," J. Opt. **15**, 075707 (2013).
11. N. Kumar, O. E. Gawhary, S. Roy, V. Kutchoukov, S. Pereira, W. Coene, and H. Urbach, "Coherent Fourier scatterometry: tool for improved sensitivity in semiconductor metrology," Proc. SPIE **8324**, 83240Q (2012).
12. V. F. Paz, S. Peterhänsel, K. Frenner, and W. Osten, "Solving the inverse grating problem by white light interference Fourier scatterometry," Light Sci. Appl. **1**, e36 (2012).
13. S. Peterhänsel, H. Laamanen, M. Kuittinen, J. Turunen, C. Pruss, W. Osten, and J. Tervo, "Solving the inverse grating problem with the naked eye," Opt. Lett. **39**, 3547–3550 (2014).
14. S. Kinoshita, S. Yoshioka, and J. Miyazaki, "Physics of structural colors," Rep. Prog. Phys. **71**, 076401 (2008).
15. J. S. Clausen, E. Højlund-Nielsen, A. B. Christiansen, S. Yazdi, M. Grajower, H. Taha, U. Levy, A. Kristensen, and N. A. Mortensen, "Plasmonic metasurfaces for coloration of plastic consumer products," Nano Lett. **14**, 4499–4504 (2014).
16. B. Tian, X. Zheng, T. J. Kempa, Y. Fang, N. Yu, G. Yu, J. Huang, and C. M. Lieber, "Coaxial silicon nanowires as solar cells and nanoelectronic power sources," Nature **449**, 885–889 (2007).
17. J. Wallentin, N. Anttu, D. Asoli, M. Huffman, I. Åberg, M. H. Magnusson, G. Siefer, P. Fuss-Kailuweit, F. Dimroth, B. Witzigmann, H. Q. Xu, L. Samuelson, K. Deppert, and M. T. Borgström, "InP nanowire array solar cells achieving 13.8% efficiency by exceeding the ray optics limit," Science **339**, 1057–1060 (2013).
18. N. Anttu, S. Lehmann, K. Storm, K. A. Dick, L. Samuelson, P. M. Wu, and M.-E. Pistol, "Crystal phase-dependent nanophotonic resonances in InAs nanowire arrays," Nano Lett. **14**, 5650–5655 (2014).
19. G. Grzela, R. Paniagua-Domínguez, T. Barten, D. van Dam, J. A. Saìnchez-Gil, and J. G. Rivas, "Nanowire antenna absorption probed with time-reversed Fourier microscopy," Nano Lett. **14**, 3227–3234 (2014).
20. P. Lalanne and E. Silberstein, "Fourier-modal methods applied to waveguide computational problems," Opt. Lett. **25**, 1092–1094 (2000).
21. M. Karamehmedović, P.-E. Hansen, K. Dirscherl, E. Karamehmedović, and T. Wriedt, "Profile estimation for Pt submicron wire on rough Si substrate from experimental data," Opt. Express **20**, 21678–21686 (2012).
22. A. M. G. Moharam, A. Pommet, E. B. Grann, and T. K. Gaylord, "Stable implementation of the rigorous coupled-wave analysis for surface relief gratings: enhanced transmittance matrix approach," J. Opt. Soc. Am. A **12**, 1077–1086 (1995).
23. B. L. Li, "Fourier modal methods for crossed anisotropic gratings with arbitrary permittivity and permeability tensors," J. Opt. A **5**, 345–355 (2003).
24. P.-E. Hansen and L. Nielsen, "Combined optimization and hybrid scalar–vector diffraction method for grating topography parameters determination," Mater. Sci. Eng. B **165**, 165–168 (2009).
25. E. D. Palik, *Handbook of Optical Constants of Solids* (Academic, 1985).
26. W. H. Press, S. A. Teukolsky, W. T. Vetterling, and B. P. Flannery, *Numerical Recipes in C++* (Cambridge University, 2002).
27. M. T. Postek, "Critical Issues in scanning electron microscope metrology," J. Res. Natl. Inst. Stand. Technol. **99**, 641–671 (1994).
28. E. Popov, M. Neviere, B. Gralak, and G. Tayeb, "Staircase approximation validity for arbitrary-shaped gratings," J. Opt. Soc. Am. A **19**, 33–42 (2002).
29. A. Savitzky and M. J. E. Golay, "Smoothing and differentiation of data by simplified least squares procedures," Anal. Chem. **36**, 1627–1639 (1964).